Ambipolar topological insulator and high-carrier mobility in solution grown ultrathin nanoplates of Sb-doped Bi_2Se_3

Zheng Ju,[a] *Yasen Hou,*[b] *Andrew Bernard,*[a] *Valentin Taufour,*[b] *Dong Yu,*[b] *and Susan M. Kauzlarich**[a]

[a] Department of Chemistry, University of California, One Shields Avenue, Davis, California 95616, United States

[b] Department of Physics, University of California, One Shields Avenue, Davis, California 95616, United States

ABSTRACT: Topological insulators (TIs) are a class of materials that can exhibit robust spin polarizations at the surfaces and have attracted much attention towards spintronic applications. Here, we optimized a solution route to synthesize ultrathin Bi_2Se_3 and Sb-doped Bi_2Se_3 nanoplates with a thickness of 6 - 15 nm and an average lateral size around 5 μm, up to a maximum of 10 μm. Solution chemistry provides high quality nanoplates of TIs with options to manipulate the surface states. We have synthesized Bi_2Se_3 and Sb-doped Bi_2Se_3 and characterized single nanoplates. Sb doping is used to suppress the bulk carriers, and an atomic percentage ~ 6% of Sb is demonstrated by energy dispersive X-ray spectroscopy (EDS). The 2D electron carrier concentration for Sb-doped Bi_2Se_3 nanoplates is lowered to 5.5×10^{12} cm^{-2}, reducing the concentration by a factor of 3 compared to the undoped Bi_2Se_3

nanoplate sample with an average 2D carrier concentration of 16 × 10^{12} cm^{-2}. At 2 K, pronounced ambipolar field effect is observed on the low-carrier-density Sb-doped Bi_2Se_3 nanoplates, further demonstrating the flexible manipulation of carrier type and concentration for these single-crystal nanoplates. Large out-of-plane magnetoresistance is measured, with a gate tunable phase coherence length.

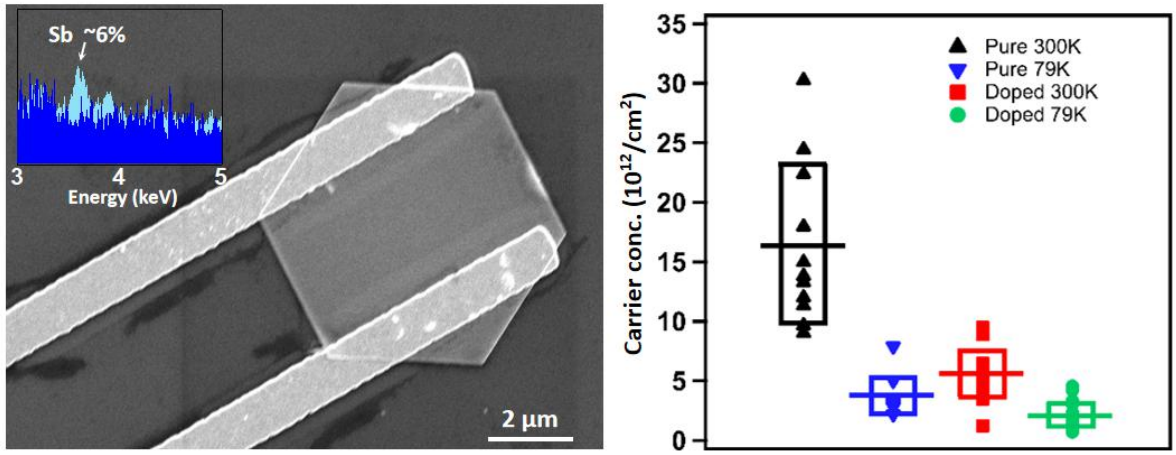

KEYWORDS: Sb-doped Bi_2Se_3, ambipolar field effect, solution synthesis, larger lateral size, magnetoresistance, low carrier concentration

INTRODUCTION:

TIs have attracted a great deal of attention due to their exotic properties and the potential for providing spin-polarization of the carriers at the surface.[1–6] Many novel applications with no analogue among traditional semiconductors are possible such as spintronic devices and new-generation electronic devices.[7,8] To date, existing theories often only consider charge/spin transport at the TI surface at the low impurity density limit. However, high density defects naturally occur in some TI materials, such as Se vacancies and interfacial defects due to surface oxidation of Bi_2Se_3.[9,10] A new mechanism predicts that moderate surface disorder can induce spin accumulation at the TI surfaces.[11] The topological nature of

the band structure leads to a transverse spin current through the bulk and spin accumulation at the surface under an external electric field.[11]

Bi_2Se_3 has been studied as a thermoelectric material[1,12–14] and a near infrared transparent conductor[15,16] and more recently as a topological insulator.[6,17] Bi_2Se_3 is of interest because of its simple surface state with a well-defined single Dirac cone and a wide bulk bandgap of 0.3 eV compared with other TIs, and thus is most promising to achieve room temperature spintronic devices. Bi_2Se_3, shown in Figure 1a, has a rhombohedral crystal structure of space group $R\bar{3}m$ ($a = b = 4.140$ Å and $c = 28.636$ Å; JCPDF #33-0214) that can be described as a layer-structure where the covalently bonded Bi_2Se_3 sheets are arranged in planar quintuple layers (QLs) of Se(1)-Bi-Se(2)-Bi-Se(1) atoms (with each QL approximately 1 nm thick). The QLs are stacked and connected by weak van der Waals interactions along the *c*-axis.

Three-dimensional TIs have typically been prepared by chemical and physical vapor deposition (CVD and PVD),[18–23] molecular beam epitaxy (MBE)[24–27] and solvothermal methods.[28–31] However, TIs prepared by CVD, PVD methods normally contain excessive bulk carriers with a comparatively higher thickness (over 30 nm).[18,20,22,24,25,32,33] Thinner TI nanostructures have been synthesized by solvothermal routes with small lateral sizes (less than 5 μm). Here, we employ a solution route[16,34] to prepare Bi_2Se_3 nanoplates with a large aspect ratio (6 - 15 nm thick and 1 - 10 μm wide). The small thickness (6 - 15 quintuple layers) reduces the bulk conductivity and allows stronger gate tunability of the Fermi level. To further suppress the bulk conductivity, Bi_2Se_3 is doped with Sb to compensate the excess electrons. Sb has been confirmed as an effective dopant which can significantly reduce carrier concentration without disrupting the topological surface state.[20,30,35] Doping Bi_2Se_3 with Sb in solution environment (without pressure as in a solvothermal environment) is more challenging than vapor deposition methods because of lower reaction temperature. However, it is a low cost, facile, and scalable method capable of producing high quality single nanoplates that allows for further chemical modification. While Sb_2Se_3 exists, it crystallizes in an orthorhombic structure rather than the Bi_2Se_3 rhombohedral crystal structure

thereby limiting the solubility of Sb in Bi_2Se_3.[36] In this manuscript, we show that a significant amount of Sb can be doped into Bi_2Se_3 via a mild solution reaction.

EXPERIMENTAL SECTION:

Pristine Bi_2Se_3 nanoplates were prepared by one pot solution synthesis following the synthesis route from Lin et.al.[16] by using bismuth nitrate pentahydrate ($Bi(NO_3)_3{\cdot}5H_2O$, 0.0970 g, ≥98%, Sigma-Aldrich), sodium selenite (Na_2SeO_3, 0.0517 g, >99%, Sigma-Aldrich) as precursors and poly(vinylpyrrolidone) (PVP, MW≈40,000, 0.22 g, Sigma-Aldrich) as surfactant in 10mL ethylene glycol (EG, Sigma-Aldrich) which serves as both solvent and reducing agent. The mixed solution was sonicated for 10 min, and then heated to 194 ℃ in a 15 mL two-neck flask equipped with thermocouple and reflux condenser in a heating mantle. To synthesize Sb-doped Bi_2Se_3, antimony acetate ($Sb(OAc)_3$, 0.0300 g, >99.5%, Sigma-Aldrich) is added with a reduced amount of $Bi(NO_3)_3{\cdot}5H_2O$ (0.0485 g), while the same synthetic procedure is carried out. After 4 hours, the heating mantle was removed, and the finished reaction was naturally cooled down to room temperature. The mixture was then centrifuged with 30 mL acetone and 10 mL isopropanol at 8500 rpm for 5 min. After the first wash, the precipitate was dispersed back into 40 mL ethanol and washed two more times. The synthesized nanoplates were then dispersed into 10 mL isopropanol for further characterization.

Powder X-ray diffraction was performed on a Bruker D8 Advance diffractometer with Cu Kα lines (40 kV, 40 mA). PXRD samples were prepared by dropcasting a small amount of the nanoplates dispersion on a fused silica holder. Electron microscopy analyses on as-synthesized Bi_2Se_3 nanoplates were performed on a Thermo Fisher Quattro S scanning electron microscopy (SEM) at an acceleration voltage at 5 kV and a JEOL JEM 2100F-AC transmission electron microscopy (TEM) at an acceleration voltage of 200 kV. TEM samples are prepared by dropcasting the suspension onto carbon films supported by Cu grids. Nanoplates lie flat on the membrane from the surface tension generated by evaporation of the isopropanol.

As-grown nanoplates in isopropanol are drop-casted onto 300 nm SiO_2 covered Si substrates, where single nanoplate field effect transistor (FET) devices were fabricated using a standard electron beam lithography process. Top metal contacts (5 nm Cr / 90 nm Au) were made using an electron beam evaporator (CHA). Current-voltage curves were measured through a current preamplifier (DL Instruments, model 1211) and a National Instruments (NI) data acquisition system. The magnetoresistance measurements were performed in a Quantum Design Physical Property Measurement System (PPMS).

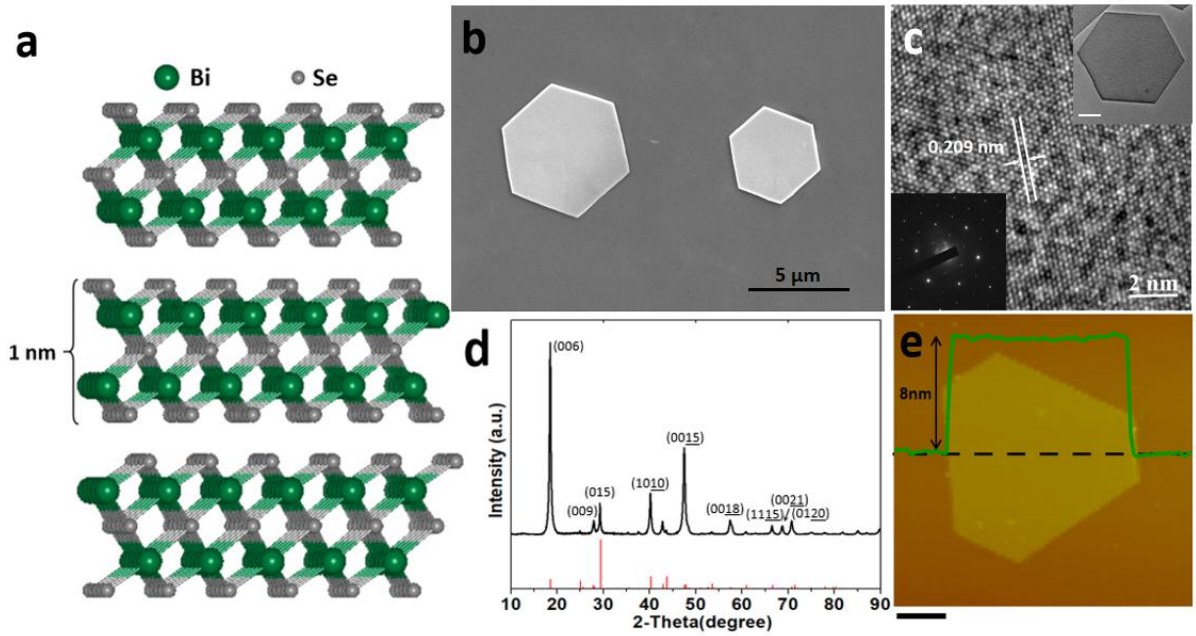

Figure 1. (a) A view of the layered rhombohedral structure of Bi_2Se_3 showing the quintuple layers (QLs) of Se(1)-Bi-Se(2)-Bi-Se(1) with a thickness around 1 nm. (b) Scanning electron microscope (SEM) image shows hexagonal shaped Bi_2Se_3 with a lateral dimension around 5 μm and 4 μm. The well resolved edge of nanoplate demonstrates the high crystallinity. (c) High resolution transmission electron microscopy (HRTEM) reveals well crystalline structure of solution synthesized Bi_2Se_3 nanoplate (top right inset) (scale bar, 1 μm). Sharp diffraction spots in the selected area diffraction pattern (bottom-left inset) further confirm the single crystal nature of nanoplate. (d) X-ray diffraction pattern of Bi_2Se_3 nanoplates with strong preferred orientation. The red bars represent characteristic reflections for rhombohedral Bi_2Se_3, PDF #33-0214. (e) Thickness of a typical solution synthesized Sb-doped Bi_2Se_3 nanoplate measured by atomic force microscopy (AFM) with a measured height of 8 nm. Scale bar, 1 μm.

RESULTS AND DISCUSSION:

The reaction to produce Bi_2Se_3 was optimized the reaction by increasing the temperature to 194 °C and extending reaction time to 4 hours to obtain nanoplates with large lateral sizes. Reaction progress was directly observed as the color of the solution changed from a colloidal white solution to dark gray to highly reflective colloidal gray precipitate, indicating the formation of Bi_2Se_3 nanoplates. The synthesized Bi_2Se_3 nanoplates are thoroughly washed by ethanol or isopropanol to remove excess surface ligands and stored as a stable colloid in isopropanol for further characterization.

Both the scanning electron microscopy (SEM) and transmission electron microscopy (TEM) images show the as-grown nanoplates typically exhibit hexagonal morphology with 120° edge facets and lateral size of 5 - 10 μm as shown in Figure 1b, 1c inset (top right) and Figure S1. The HRTEM image reveals the single-crystalline nature of the nanoplate (Figure 1c), also confirmed by the selected area electron diffraction (SAED) pattern Figure 1c inset (bottom left). The lattice spacing in HRTEM is ~0.209 nm corresponding to the (11-20) plane. The phase purity of the products was characterized by X-ray diffraction (XRD). As indicated in Figure 1d, the nanoplates obtained by this solution route display a pure rhombohedral phase of Bi_2Se_3 with a space group $R\bar{3}m$. All the major peaks can be indexed to (0001) family and the larger than calculated intensity for the *l* Miller index direction is due to preferred alignment of the nanoplates. The calculated lattice constants of $a = b = 4.153(5)$ Å and $c = 28.612(9)$ Å are in good agreement with the standard literature values ($a = b = 4.140$ Å and $c = 28.636$ Å; JCPDF #33-0214). For the synthesis of Sb-doped Bi_2Se_3, excess Sb precursor was added to overcome the limited solubility in Bi_2Se_3 rhombohedral structure. The final product contains unreacted Se impurity and no other possible impurities such as the orthorhombic form of Bi_2Se_3,[37,38] according to the XRD of the product from the reaction (See Supporting Information, Figure S2). The thicknesses of the doped Bi_2Se_3 nanoplates are measured by atomic force microscopy (AFM) and range from 6 to 15 nm. Figure 1e shows an AFM image of a typical nanoplate with a smooth surface, which further demonstrates the surface ligands, such as PVP, have been successfully removed by the washing process.

The energy dispersive spectroscopy (EDS) spectrum obtained for an undoped Bi_2Se_3 single nanoplate shows stoichiometry of Bi:Se ~2:3 (Figure 2a), confirming the composition. The EDS spectrum from a single Sb-doped nanoplate shows an Sb atomic percentage of ~ 6% (Figure 2b), which is significantly increased compared to nanoplates obtained from solvothermal synthesis,[30] and close to that of vapor-phase-synthesized nanoribbon (~ 7%).[20] We found that the amount of Sb in various nanoplates ranged from 3-6% from the same batch. Further efforts are necessary to ensure a consistent maximum doping of the nanoplates. EDS elemental mapping reveals Se, Bi and Sb are evenly distributed across the entire nanoplate (Figure 2c).

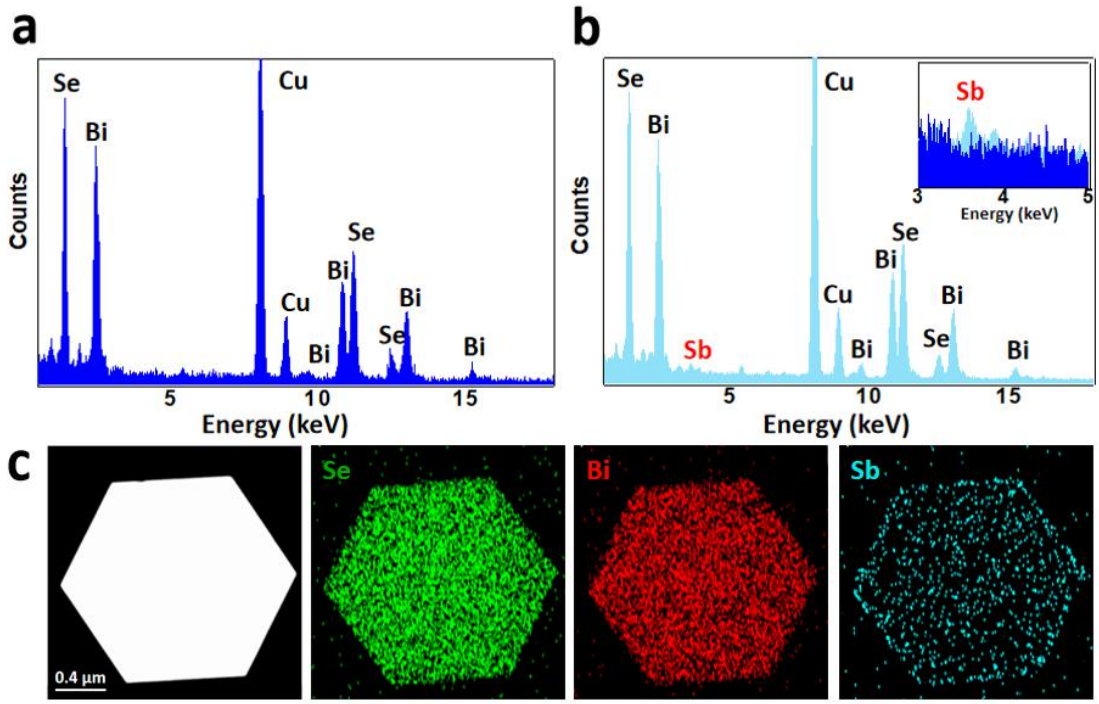

Figure 2. (a) EDS spectrum under TEM of a single Bi_2Se_3 nanoplate. (b) EDS spectrum of a Sb-doped Bi_2Se_3 single nanoplate. Inset shows the stacked EDS spectra of Sb-doped and undoped Bi_2Se_3 showing a noticeable Sb peak in Sb-doped sample, corresponding to an atomic concentration of ~6%. Copper signal is from TEM sample grid. (c) Dark-field scanning transmission electron microscopy (DF-STEM) image and EDS elemental mapping of selenium, bismuth and antimony on one Sb-doped Bi_2Se_3 nanoplate, indicating a uniform distribution of the elements.

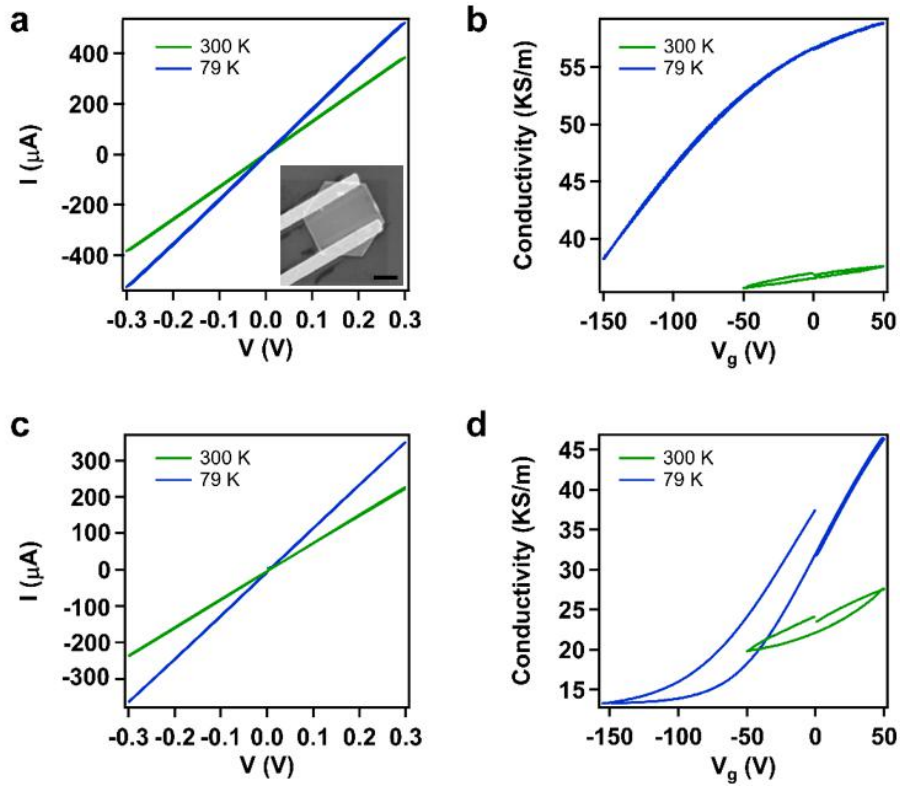

Figure 3. Field effect characteristics of undoped and Sb doped Bi_2Se_3 devices. (a) I-V curves for a typical undoped Bi_2Se_3 device (#1) at 300 K and 79 K. Inset is the SEM image of a typical device. Two bright bars are top metal contacts (5 nm Cr / 90 nm Au) deposited on single nanoplate. Scale bar, 2 μm. (b) Gate dependence of conductance at 300 K and 79 K. Field-effect mobility and electron concentration are estimated to be $\mu = 33$ cm^2/Vs, $n_{2D} = 14 \times 10^{12}$ cm^{-2} at 300 K and $\mu = 249$ cm^2/Vs, $n_{2D} = 3 \times 10^{12}$ cm^{-2} at 79 K. (c)-(d) I-V curves and gate dependent conductance for Sb doped Bi_2Se_3 (device #2). Field-effect mobility and electron concentration are estimated to be $\mu = 56$ cm^2/Vs, $n_{2D} = 4.82 \times 10^{12}$ cm^{-2} at 300 K and $\mu = 494$ cm^2/Vs, $n_{2D} = 0.82 \times 10^{12}$ cm^{-2} at 79 K.

Electronic measurements of single nanoplate field effect transistors (FETs) with undoped (device #1) and Sb doped (device #2) Bi_2Se_3 are shown in Figure 3. Both devices show linear current-voltage (I-V) curves which indicate ohmic conduction and are more conductive at liquid nitrogen temperature (Figure 3a and 3c). Conductivity of device #2 shows a strong temperature dependence as shown in Figure S3. Contact resistance determined by 3-probe measurements is well below 100 Ω (Figure S4). Gate dependence at room temperature indicates both undoped and Sb doped are *n*-type (Figure 3b and 3d). The carrier concentration of undoped Bi_2Se_3 is double that of Sb doped Bi_2Se_3. As the temperature is

lowered to 79K, both devices show stronger gate response (Figure 3b and 3d). We then extract the field effect mobility and carrier concentration by using a parallel plate capacitance model. Note that this model only provides an estimation of the exact mobility value, because of the fringe effects near the metal contact and the often-irregular shapes of the nanoplate channels. The possible field screening at the SiO_2 nanoplate interface may also lead to an underestimation of the mobility. From this model, the 2D carrier concentration in the Sb doped Bi_2Se_3 nanoplate is as low as 0.82×10^{12} cm^{-2}.

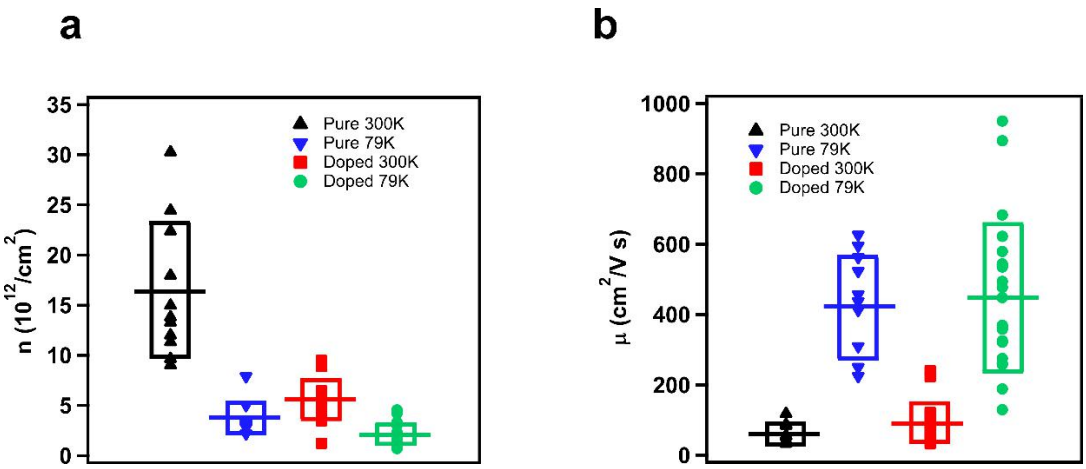

Figure 4. (a) Distribution of electron concentration and (b) field effect mobility of undoped and Sb doped Bi_2Se_3 nanoplate devices at 300K and 79K respectively. The horizontal lines indicate the average and the boxes indicate the standard deviation. Sb-doping effectively lowered the electron concentration by half at both 300K and 79K.

To further confirm the doping effects, we measured 11 undoped Bi_2Se_3 and 19 Sb-doped Bi_2Se_3 single nanoplate devices. Statistics of carrier mobility and concentration are shown in Figure 4 and Table S1. On average, as-prepared undoped Bi_2Se_3 nanoplates have a mobility μ = 60.4 cm^2/Vs and carrier concentration $n_{2D} = 16.3 \times 10^{12}$ cm^{-2} at 300 K, while Sb doped Bi_2Se_3 nanoplates have a mobility μ = 93.5 cm^2/Vs and carrier concentration $n_{2D} = 5.5 \times 10^{12}$ cm^{-2}. At low temperature, the field-effect mobility in both types of devices increases greatly up to 10^3 cm^2/Vs for the best devices and the carrier concentration is further reduced. Our data clearly demonstrate that by Sb doping, the carrier concentration of Bi_2Se_3 can be effectively reduced.

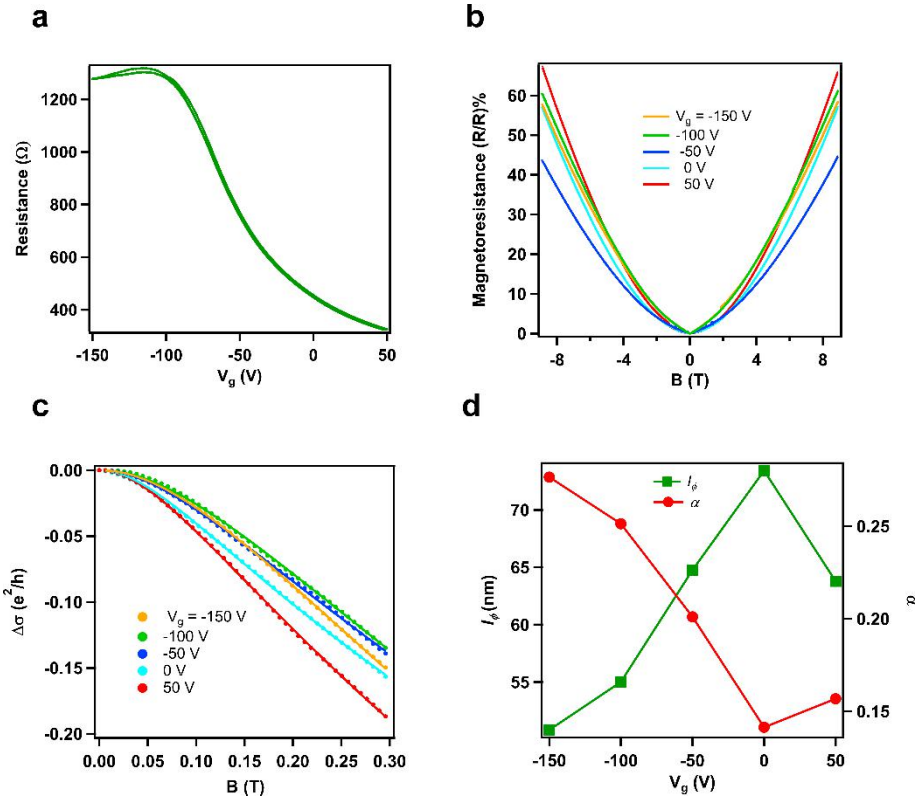

Figure 5. (a) Gate voltage dependence of resistance of device #2 at 2 K, which indicates ambipolar conduction. (b) Magnetoresistance of device #2 as a function of out-of-plane magnetic field at various gate voltages at 2 K. (c) Magneto-conductance as a function of magnetic field. Solid lines are fitting curves with the HLN equation. (d) α and phase coherence length l_Φ at different gate voltages. The error bars from fitting are smaller than the size of the data points

We attribute the lower carrier concentration in Sb doped Bi_2Se_3 to less Se vacancies. Bi_2Se_3 is a heavily doped n-type semiconductor because of the non-stoichiometric composition with a slight deficiency of Se.[30,39,40] The lower carrier concentration in Sb-doped Bi_2Se_3 allows for the observation of an ambipolar gate response in at 2K (Figure 5). As gate voltage is scanned to -150 V, the device resistance first increases due to the reduction of electron concentration. Maximum resistance is observed at -117 V. As the gate voltage continues to decrease, resistance of the device decreases because of the increasing hole conduction. The gate response is much weaker in the p-type regime as seen in Figure 5a. This is not understood but may be caused by lower hole mobility and/or stronger field screening at high gate voltage.

The device thickness of this nanoplate is only around 12 nm. It is likely that both top and bottom surfaces are affected by the gate simultaneously.[20] The ambipolar gate response clearly indicates that we can effectively tune the Fermi level from above the Dirac point to below it. Electron concentration as low as $n_{2D} = 3.1\times10^{11}/cm^2$ at V_g = -117 V has been realized in this device. This estimated carrier concentration consists of both surface and bulk contributions. The value is comparable with the reported lowest carrier concentrations measured in Bi_2Se_3.[20,41] Such low carrier concentration is essential to minimize bulk transport of TI materials and provides a possible way to study the surface transport of Bi_2Se_3.

Magnetoresistance (MR) measurements are also performed on this device (#2). As can be seen in Figure 5b, positive MR responses are observed under all gate voltages, showing weak anti-localization, which is in consistence with the strong spin-orbital coupling in Sb doped Bi_2Se_3. MR as large as 60% is observed at 9 T. According to the Hikami-Larkin-Nagaoka (HLN) theory, for a 2D system, the magneto-conductivity ($\Delta\sigma = \sigma(B) - \sigma(B = 0)$) is given as follows[42]:

$$\Delta\sigma = \alpha\frac{e^2}{2\pi^2\hbar}\left[\ln\frac{\hbar}{4el_\Phi^2B} - \psi\left(\frac{1}{2}+\frac{\hbar}{4el_\Phi^2B}\right)\right] \qquad (1)$$

where l_Φ is the phase coherence length, Ψ is the digamma function, $\hbar$ is the reduced Plank's constant, and α is a fitting parameter that takes a value of 1/2 for a 2D system with strong spin-orbit coupling or the surface of a 3D topological insulator.[42-44] The $\Delta\sigma$ data can be fit with the HLN equation very well under all gate voltages (Figure 5c). Phase coherence length extracted from the fitting is around 65 nm, close to previously reported values.[45-48] α obtained from the fitting is around 0.26, which is a value similar to previous studies[43-45,49] and in rough agreement with the symplectic limit. The deviation from 1/2 has been generally attributed to the intermixing between the bulk and surface states[47-50] or sample inhomogeneity.[43] Additionally, the existence of contact resistance may also lead to an underestimation of the fitting parameters.

CONCLUSION:

In summary, an optimized solution method is utilized to prepare Sb-doped Bi_2Se_3 nanoplates with a lateral size up to 10 μm and as high as 6% doping amount which is close to that of vapor-phase or solvothermal synthesized samples. Sb-doping of Bi_2Se_3 successfully reduced the electron concentration both at room temperature (300 K) and liquid nitrogen temperature (79 K), compared with undoped Bi_2Se_3 nanoplates. A pronounced ambipolar field effect is observed in the Sb-doped Bi_2Se_3 sample, indicating successful Sb incorporation and flexibility to manipulate the Fermi level from above to below the Dirac point. Magnetoresistance up to 60% is observed in ambipolar devices where the phase coherent length is around 10 nm. The solution synthesis of high-quality Sb-doped Bi_2Se_3 nanoplates offers an option for chemically manipulating topological insulators and exploring the properties of single nanoplates with applications in photoelectric[51] and spintronic areas.

ASSOCIATED CONTENT

Supporting information

SEM image of large lateral size Bi_2Se_3 nanoplate; XRD pattern of Sb-doped Bi_2Se_3 sample; Temperature dependent conductivity of Sb-doped Bi_2Se_3 device; Contact resistance of 3 probe measurements; Table of statistics of carrier concentration and field effect mobility of undoped and Sb doped Bi_2Se_3 devices.

Funding Sources

Financial support from the NSF (DMR-1709382, DMR-1838532) is gratefully acknowledged. The Advanced Materials Characterization and Testing Lab (AMCaT) of University of California Davis is acknowledged for providing characterization facilities.

REFERENCES:

(1) Kong, D.; Cui, Y. Opportunities in Chemistry and Materials Science for Topological Insulators and Their Nanostructures. *Nature Chemistry*. **2011**, *3*, 845–849.

(2) Qi, X. L.; Zhang, S. C. Topological Insulators and Superconductors. *Rev. Mod. Phys.* **2011**, *83* (4), 1057.

(3) Moore, J. E. The Birth of Topological Insulators. *Nature*. **2010**, *464*, 194–198.

(4) Müchler, L.; Zhang, H.; Chadov, S.; Yan, B.; Casper, F.; Kübler, J.; Zhang, S. C.; Felser, C. Topological Insulators from a Chemist's Perspective. *Angew. Chemie - Int. Ed.* **2012**, *51* (29), 7221–7225.

(5) Hasan, M. Z.; Kane, C. L. Colloquium: Topological Insulators. *Rev. Mod. Phys.* **2010**, *82* (4), 3045–3067.

(6) Zhang, H.; Liu, C. X.; Qi, X. L.; Dai, X.; Fang, Z.; Zhang, S. C. Topological Insulators in Bi_2Se_3, Bi_2Te_3 and Sb_2Te_3 with a Single Dirac Cone on the Surface. *Nat. Phys.* **2009**, *5* (6), 438–442.

(7) Žutić, I.; Fabian, J.; Das Sarma, S. Spintronics: Fundamentals and Applications. *Rev. Mod. Phys.* **2004**, *76* (2), 323–410.

(8) Pesin, D.; MacDonald, A. H. Spintronics and Pseudospintronics in Graphene and Topological Insulators. *Nat. Mater.* **2012**, *11* (5), 409–416.

(9) Yashina, L. V.; Sánchez-Barriga, J.; Scholz, M. R.; Volykhov, A. A.; Sirotina, A. P.; Neudachina, V. S.; Tamm, M. E.; Varykhalov, A.; Marchenko, D.; Springholz, G.; Bauer, G.; Knop-Gericke, A.; Rader, O. Negligible Surface Reactivity of Topological Insulators Bi_2Se_3 and Bi_2Te_3 towards Oxygen and Water. *ACS Nano* **2013**, *7* (6), 5181–5191.

(10) Kong, D.; Cha, J. J.; Lai, K.; Peng, H.; Analytis, J. G.; Meister, S.; Chen, Y.; Zhang, H. J.; Fisher,

I. R.; Shen, Z. X.; Cui, Y. Rapid Surface Oxidation as a Source of Surface Degradation Factor for Bi_2Se_3. *ACS Nano* **2011**, *5* (6), 4698–4703.

(11) Peng, X.; Yang, Y.; Singh, R. R. P.; Savrasov, S. Y.; Yu, D. Spin Generation via Bulk Spin Current in Three-Dimensional Topological Insulators. *Nat. Commun.* **2016**, *7*, 10878.

(12) Tretiakov, O. A.; Abanov, A.; Murakami, S.; Sinova, J. Large Thermoelectric Figure of Merit for Three-Dimensional Topological Anderson Insulators via Line Dislocation Engineering. *Appl. Phys. Lett.* **2010**, *97* (7), 073108.

(13) Ghaemi, P.; Mong, R. S. K.; Moore, J. E. In-Plane Transport and Enhanced Thermoelectric Performance in Thin Films of the Topological Insulators Bi_2Te_3 and Bi_2Se_3. *Phys. Rev. Lett.* **2010**, *105* (16), 166603.

(14) Wang, S.; Sun, Y.; Yang, J.; Duan, B.; Wu, L.; Zhang, W.; Yang, J. High Thermoelectric Performance in Te-Free $(Bi,Sb)_2Se_3$: Via Structural Transition Induced Band Convergence and Chemical Bond Softening. *Energy Environ. Sci.* **2016**, *9* (11), 3436–3447.

(15) Peng, H.; Dang, W.; Cao, J.; Chen, Y.; Wu, D.; Zheng, W.; Li, H.; Shen, Z. X.; Liu, Z. Topological Insulator Nanostructures for Near-Infrared Transparent Flexible Electrodes. *Nat. Chem.* **2012**, *4* (4), 281–286.

(16) Lin, Z.; Chen, Y.; Yin, A.; He, Q.; Huang, X.; Xu, Y.; Liu, Y.; Zhong, X.; Huang, Y.; Duan, X. Solution Processable Colloidal Nanoplates as Building Blocks for High-Performance Electronic Thin Films on Flexible Substrates. *Nano Lett.* **2014**, *14* (11), 6547–6553.

(17) Xia, Y.; Qian, D.; Hsieh, D.; Wray, L.; Pal, A.; Lin, H.; Bansil, A.; Grauer, D.; Hor, Y. S.; Cava, R. J.; Hasan, M. Z. Observation of a Large-Gap Topological-Insulator Class with a Single Dirac Cone on the Surface. *Nat. Phys.* **2009**, *5* (6), 398–402.

(18) Kong, D.; Dang, W.; Cha, J. J.; Li, H.; Meister, S.; Peng, H.; Liu, Z.; Cui, Y. Few-Layer Nanoplates of Bi_2Se_3 and Bi_2Te_3 with Highly Tunable Chemical Potential. *Nano Lett.* **2010**, *10* (6), 2245–2250.

(19) Cao, H.; Venkatasubramanian, R.; Liu, C.; Pierce, J.; Yang, H.; Zahid Hasan, M.; Wu, Y.; Chen, Y. P. Topological Insulator Bi_2Te_3 Films Synthesized by Metal Organic Chemical Vapor Deposition. *Appl. Phys. Lett.* **2012**, *101* (16), 162104.

(20) Hong, S. S.; Cha, J. J.; Kong, D.; Cui, Y. Ultra-Low Carrier Concentration and Surface-Dominant Transport in Antimony-Doped Bi_2Se_3 Topological Insulator Nanoribbons. *Nat. Commun.* **2012**, *3*, 757.

(21) Guo, Y.; Aisijiang, M.; Zhang, K.; Jiang, W.; Chen, Y.; Zheng, W.; Song, Z.; Cao, J.; Liu, Z.; Peng, H. Selective-Area van Der Waals Epitaxy of Topological Insulator Grid Nanostructures for Broadband Transparent Flexible Electrodes. *Adv. Mater.* **2013**, *25* (41), 5959–5964.

(22) Brom, J. E.; Ke, Y.; Du, R.; Won, D.; Weng, X.; Andre, K.; Gagnon, J. C.; Mohney, S. E.; Li, Q.; Chen, K.; Xi, X. X.; Redwing, J. M. Structural and Electrical Properties of Epitaxial Bi_2Se_3 Thin Films Grown by Hybrid Physical-Chemical Vapor Deposition. *Appl. Phys. Lett.* **2012**, *100* (16), 162110.

(23) Xu, Z.; Guo, X.; Yao, M.; He, H.; Miao, L.; Jiao, L.; Liu, H.; Wang, J.; Qian, D.; Jia, J.; Ho, W.; Xie, M. Anisotropic Topological Surface States on High-Index Bi_2Se_3 Films. *Adv. Mater.* **2013**, *25* (11), 1557–1562.

(24) Liu, X.; Smith, D. J.; Fan, J.; Zhang, Y. H.; Cao, H.; Chen, Y. P.; Leiner, J.; Kirby, B. J.; Dobrowolska, M.; Furdyna, J. K. Structural Properties of Bi_2Te_3 and Bi_2Se_3 Topological Insulators Grown by Molecular Beam Epitaxy on GaAs(001) Substrates. *Appl. Phys. Lett.* **2011**, *99* (17), 171903.

(25) Schreyeck, S.; Tarakina, N. V.; Karczewski, G.; Schumacher, C.; Borzenko, T.; Brüne, C.; Buhmann, H.; Gould, C.; Brunner, K.; Molenkamp, L. W. Molecular Beam Epitaxy of High Structural Quality Bi_2Se_3 on Lattice Matched InP(111) Substrates. *Appl. Phys. Lett.* **2013**, *102* (4), 041914.

(26) Zhang, Y.; He, K.; Chang, C. Z.; Song, C. L.; Wang, L. L.; Chen, X.; Jia, J. F.; Fang, Z.; Dai, X.; Shan, W. Y.; Shen, S. Q.; Niu, Q.; Qi, X. L., Zhang, S. C.; Ma, X. C.; Xue Q. K. Crossover of the Three-Dimensional Topological Insulator Bi_2Se_3 to the Two-Dimensional Limit. *Nat. Phys.* **2010**, *6* (8), 584–588.

(27) Li, Y. Y.; Wang, G.; Zhu, X. G.; Liu, M. H.; Ye, C.; Chen, X.; Wang, Y. Y.; He, K.; Wang, L. L.; Ma, X. C.; Zhang, H. J.; Dai, X.; Fang, Z.; Xie, X. C.; Liu, Y.; Qi, X. L.; Jia, J. F.; Zhang S. C.; Xue, Q. K. Intrinsic Topological Insulator Bi_2Te_3 Thin Films on Si and Their Thickness Limit. *Adv. Mater.* **2010**, *22* (36), 4002–4007.

(28) Yang, L.; Chen, Z. G.; Hong, M.; Han, G.; Zou, J. Enhanced Thermoelectric Performance of Nanostructured Bi_2Te_3 through Significant Phonon Scattering. *ACS Appl. Mater. Interfaces* **2015**, *7* (42), 23694–23699.

(29) Zhang, G.; Wang, W.; Lu, X.; Li, X. Solvothermal Synthesis of V-VI Binary and Ternary Hexagonal Platelets: The Oriented Attachment Mechanism. *Cryst. Growth Des.* **2009**, *9* (1), 145–150.

(30) Kong, D.; Koski, K. J.; Cha, J. J.; Hong, S. S.; Cui, Y. Ambipolar Field Effect in Sb-Doped Bi_2Se_3 Nanoplates by Solvothermal Synthesis. *Nano Lett.* **2013**, *13* (2), 632–636.

(31) Liu, X.; Xu, J.; Fang, Z.; Lin, L.; Qian, Y.; Wang, Y.; Ye, C.; Ma, C.; Zeng, J. One-Pot Synthesis of Bi_2Se_3 Nanostructures with Rationally Tunable Morphologies. *Nano Res.* **2015**, *8* (11), 3612–3620.

(32) Andzane, J.; Kunakova, G.; Charpentier, S.; Hrkac, V.; Kienle, L.; Baitimirova, M.; Bauch, T.; Lombardi, F.; Erts, D. Catalyst-Free Vapour-Solid Technique for Deposition of Bi_2Te_3 and Bi_2Se_3 Nanowires/Nanobelts with Topological Insulator Properties. *Nanoscale* **2015**, *7* (38), 15935–15944.

(33) Kunakova, G.; Galletti, L.; Charpentier, S.; Andzane, J.; Erts, D.; Léonard, F.; Spataru, C. D.; Bauch, T.; Lombardi, F. Bulk-Free Topological Insulator Bi_2Se_3 Nanoribbons with Magnetotransport Signatures of Dirac Surface States. *Nanoscale* **2018**, *10* (41), 19595–19602.

(34) Soni, A.; Yanyuan, Z.; Ligen, Y.; Aik, M. K. K.; Dresselhaus, M. S.; Xiong, Q. Enhanced Thermoelectric Properties of Solution Grown $Bi_2Te_{3-x}Se_x$ Nanoplatelet Composites. *Nano Lett.* **2012**, *12* (3), 1203–1209.

(35) Zhang, Y.; Chang, C. Z.; He, K.; Wang, L. L.; Chen, X.; Jia, J. F.; Ma, X. C.; Xue, Q. K. Doping Effects of Sb and Pb in Epitaxial Topological Insulator Bi_2Se_3 Thin Films: An in Situ Angle-Resolved Photoemission Spectroscopy Study. *Appl. Phys. Lett.* **2010**, *97* (19), 194102.

(36) Kong, D.; Chen, Y.; Cha, J. J.; Zhang, Q.; Analytis, J. G.; Lai, K.; Liu, Z.; Hong, S. S.; Koski, K. J.; Mo, S. K.; Hussain, Z.; Fisher, I. R.; Shen, Z. X.; Cui, Y. Ambipolar Field Effect in the Ternary Topological Insulator $(Bi_xSb_{1-x})_2Te_3$ by Composition Tuning. *Nat. Nanotechnol.* **2011**, *6* (11), 705–709.

(37) Patil, N. S.; Sargar, A. M.; Mane, S. R.; Bhosale, P. N. Growth Mechanism and Characterisation of Chemically Grown Sb Doped Bi_2Se_3 Thin Films. *Appl. Surf. Sci.* **2008**, *254* (16), 5261-5265.

(38) Qiu, X.; Burda, C.; Fu, R.; Pu, L.; Chen, H.; Zhu, J. Heterostructured Bi_2Se_3 Nanowires with Periodic Phase Boundaries. *J. Am. Chem. Soc.* **2004**, *126* (50), 16276-16277.

(39) Köhler, H. Conduction Band Parameters of Bi_2Se_3 from Shubnikov-de Haas Investigations. *Phys. Status Solidi* **1973**, *58* (1), 91–100.

(40) Analytis, J. G.; Chu, J. H.; Chen, Y.; Corredor, F.; McDonald, R. D.; Shen, Z. X.; Fisher, I. R. Bulk Fermi Surface Coexistence with Dirac Surface State in Bi_2Se_3: A Comparison of Photoemission and Shubnikov-de Haas Measurements. *Phys. Rev. B - Condens. Matter Mater. Phys.* **2010**, *81* (20), 205407.

(41) Lang, M.; He, L.; Xiu, F.; Yu, X.; Tang, J.; Wang, Y.; Kou, X.; Jiang, W.; Fedorov, A. V.; Wang, K. L. Revelation of Topological Surface States in Bi_2Se_3 Thin Films by in Situ Al Passivation. *ACS Nano* **2012**, *6* (1), 295–302.

(42) Hikami, S.; Larkin, A. I.; Nagaoka, Y. Spin-Orbit Interaction and Magnetoresistance in the Two Dimensional Random System. *Prog. Theor. Phys.* **2005**, *63* (2), 707–710.

(43) Chen, J.; Qin, H. J.; Yang, F.; Liu, J.; Guan, T.; Qu, F. M.; Zhang, G. H.; Shi, J. R.; Xie, X. C.; Yang, C. L.; Wu, K. H.; Li, Y. Q.; Lu, L. Gate-Voltage Control of Chemical Potential and Weak Antilocalization in Bi_2Se_3. *Phys. Rev. Lett*. **2010**, 105 (17), 176602.

(44) Matsuo, S.; Koyama, T.; Shimamura, K.; Arakawa, T.; Nishihara, Y.; Chiba, D.; Kobayashi, K.; Ono, T.; Chang, C. Z.; He, K.; Ma, X. C.; Xue, Q. K. Weak Antilocalization and Conductance Fluctuation in a Submicrometer-Sized Wire of Epitaxial Bi_2Se_3. *Phys. Rev. B - Condens. Matter Mater. Phys.* **2012**, 85 (7), 075440.

(45) Liu, M.; Chang, C. Z.; Zhang, Z.; Zhang, Y.; Ruan, W.; He, K.; Wang, L. L.; Chen, X.; Jia, J. F.; Zhang, S. C.;Xue, Q. K.; Ma, X. C.; Wang, Y. Electron Interaction-Driven Insulating Ground State in Bi_2Se_3 Topological Insulators in the Two-Dimensional Limit. *Phys. Rev. B - Condens. Matter Mater. Phys.* **2011**, 83 (16), 165440.

(46) Tian, J.; Chang, C.; Cao, H.; He, K.; Ma, X.; Xue, Q.; Chen, Y. P. Quantum and Classical Magnetoresistance in Ambipolar Topological Insulator Transistors with Gate-Tunable Bulk and Surface Conduction. *Sci. Rep.* **2014**, 4, 4859.

(47) Cha, J. J.; Kong, D.; Hong, S. S.; Analytis, J. G.; Lai, K.; Cui, Y. Weak Antilocalization in $Bi_2(Se_xTe_{1-x})_3$ Nanoribbons and Nanoplates. Nano Lett. **2012**, 12 (2), 1107–1111.

(48) Steinberg, H.; Laloë, J. B.; Fatemi, V.; Moodera, J. S.; Jarillo-Herrero, P. Electrically Tunable Surface-to-Bulk Coherent Coupling in Topological Insulator Thin Films. *Phys. Rev. B - Condens. Matter Mater. Phys*. **2011**, 84 (23), 233101.

(49) Wang, Z.; Yang, L.; Zhao, X.; Zhang, Z.; Gao, X. P. A. Linear Magnetoresistance versus Weak Antilocalization Effects in Bi_2Te_3. *Nano Res.* **2015**, 8 (9), 2963–2969.

(50) Chen, J.; He, X. Y.; Wu, K. H.; Ji, Z. Q.; Lu, L.; Shi, J. R.; Smet, J. H.; Li, Y. Q. Tunable Surface Conductivity in Bi_2Se_3 Revealed in Diffusive Electron Transport. *Phys. Rev. B - Condens. Matter Mater. Phys.* **2011**, 83 (24), 241304.

(51) Zhang, H.; Zhang, X.; Liu, C.; Lee, S. T.; Jie, J. High-Responsivity, High-Detectivity, Ultrafast Topological Insulator Bi_2Se_3/Silicon Heterostructure Broadband Photodetectors. *ACS Nano* **2016**, *10* (5), 5113–5122.